Acceleration of glacier mass lost after ~2013 at the Mt. Everest (Qomolangma)

LI Gang[1], LIN Hui[1, 2, 3], YE Qinghua[4], JIANG Liming[5], HOOPER Andrew[6]

1. *Institute of Space and Earth Information Science, The Chinese University of Hong Kong, Hong Kong, China*;
2. *Geography and Resource Management, The Chinese University of Hong Kong, Hong Kong, China*;
3. *School of Geography and Environment, Jiangxi Normal University, Nanchang* 330022*, China*;
4. *Institute of Tibetan Plateau Research, Chinese Academic of Science, Beijing* 100100*, China*;
5. *Institute of Geodesy and Geophysics, Chinese Academy of Science, Wuhan* 430077*, China*;
6. *COMET, School of Earth and Environment, University of Leeds, United Kingdom.*

Abstract: Satellite geodesy is capable for observing glacier height changes and most recent studies focus on the decadal scale due to limitations of data acquisition and precision. Glaciers at Mt. (Qomolangma), locating at the Central Himalaya, have been studies from the 1970s to 2015. Here we obtained TerraSAR-X/TanDEM-X images observed in two epochs, a group around 2013 and another in 2017. Together with SRTM observed in 2000, we derived glacier geodetic glacier mass balance between 2000 and ~2013 and ~2013 and 2017. We proposed two InSAR procedures for deriving the second period, which yield with basically identical results of geodetic glacier mass balance. DEMs differencing between DEMs derived by TerraSAR-X/TanDEM-X show better precision than between TerraSAR-X/TanDEM-X formed DEM and SRTM, and are capable of providing geodetic glacier mass balance at sub-decadal scale. Glaciers at the Mt. Everest and its surroundings present obvious speeding up in mass lost rates before and after ~2013 for both the Chinese and the Nepalese sides. The previous obtained spatial heterogeneous pattern for glacier downwasting between 2000 and ~2013 generally kept the same after ~2013. Glaciers with lacustrine terminus present most rapid lost rates.

Key words: Everest; Qomolangma; Geodetic glacier mass balance; TerraSAR-X/TanDEM-X; Bistatic D-InSAR

Citation format: Li G,Lin H,Ye Q H,Jiang L M and Hooper A. 2020. Acceleration of glacier mass lost after ~2013 at the Mt. Everest (Qomolangma). Journal of Remote Sensing(Chinese). 24(S1): 132−139

1 INTRODUCKTION

Mt. Everest (Qomolangma), locates at Central Himalaya, is the highest peak in the world. Glaciers in Himalaya and its surroundings experienced accelerating mass loss in last few decades (Maurer, et al., 2019). Given their fame, these glaciers gather great interests of researches. As one of the hot-spotted study regions, Mt. Everest and its surroundings have geodetic glacier mass balance records spanning from the 1970s to recent years, which generally indicates more negative rates trend despite their different observation sensors or platforms including stereo photogrammetry, SAR interferometry, and laser altimetry (Bolch, et al., 2011; Kääb, et al., 2015; Ye, et al., 2015; King, et al., 2017; Li, et al., 2018). Supra-glacial lake expansion also indicates a similar glacier mass lost accelerating trend (Ye, et al., 2009). For the period after 2000, most of these researches regarded it as one stage or study period. ICESat derived glacier mass balance between 2003 - 2009 was -0.37 ± 0.10 m w. e. (water equivalent)/a, TerraSAR-X/TanDEM-X (TSX/TDX) - SRTM derived result was -0.38 ± 0.04 m w. e./a for 2000 - ~2012, and WorldView - SRTM derived result was -0.52 ± 0.22 m w. e./a. Consider this period is longer than one decade, it is necessary to study the changes or fluctuation within this period. The previous study also indicated a heterogeneity map of glacier mass balance which possibly induced by debris-covering rate, terminating types, temperature rising rates, and glacier flow rates (Li, et al., 2018).

Most of the current geodetic glacier mass balance studies focused at decadal scale and even longer study period over the High-mountains Asia (HMA). Since the precision of deriving geodetic glacier mass balance depends on the accuracy of forming a Digital Elevation Model (DEMs), a pair of relatively rough DEMs that observed with one-decade temporal baseline or longer could be capable to derive glacier height changes at acceptable precision because of averaging reduces the annual error. If aiming at deriving glacier mass balance for sub-decadal scale and/or annual scale, the precision of DEMs is highly demanded. The absolute vertical accuracy of SRTM is ±16m (90% confidence interval), and accuracy of TanDEM-X DEM (DEM formed by TSX/TDX interferometry) is 2m (Farr, et al., 2007; Krieger, et al., 2013). Consider that the differencing operation between SRTM and TanDEM-X DEM usually gives vertical RMSE at better than 5m, the datum error could be the major error in the total error of these DEMs (Li and Lin 2017;

Received: XXXX-XX-XX; **Accepted:** XXXX-XX-XX

First author biography: biography: LI Gang (1986—), male, Pos-Doc, he interests in satellite imagery geodesy, cryospheric remote sensing and modelling, Email: ligang@link.cuhk.edu.hk

Corresponding author biography: LIN Hui (1954—), male, Professor, he interests in includes satellite remote sensing, Virtual Geographic Environments (VGE), Email: huilin@cuhk.edu.hk

Li, et al., 2018). Consider another research by comparing SRTM and SPOT images formed DEM usually gives vertical RMSE worse than 8m at similar study sites (Gardelle, et al., 2013), the precision of TanDEM DEM should be better than the SPOT DEM. Given its high precision, in this study we seek to explore the capability of deriving sub-decadal glacier mass balance by using multi acquisitions of bistatic TSX/TDX observed at different points of time. One study applied two epochs of TSX/TDX observation and derived geodetic glacier mass balance at Puruogangri Ice Field in northern Tibetan Plateau (Liu, et al., 2016). Their standard deviation of DEM difference map at the off-glacier area was 2.28 m by comparing two TanDEM-X DEMs observed in 2012 and 2016. Consider that the topography at the Mt. Everest is much steeper at the Puruogangri, deriving sub-decadal geodetic glacier mass balance for the Mt. Everest should be a challenge.

2 STUDY SITE

Mt. Everest, the highest summit of the world, locates in the Central Himalaya along the border between China and Nepal at the maximum height of 8844.43m (Ye, et al., 2015). The main ridge is the national border adjacent to the Mt. Everest (Fig 1). The study area of this research basically overlaps Li, et al.' research (2018). According to Randolph glacier inventory (RGI) v5.0 (RGI Consortium, 2015), glaciers cover for 1708.2 km^2 at our study site (86°18' ~ 87°28'E, 27°36' ~ 28°24'N). The lowest glacier terminus found at 3718 m for Kazhenpu Glacier. Following Li, et al.'s research (2018), we separate our study sites into eight sub-regions according to topography, debris covering rates and the study sites of several previous published studies (Bolch, et al., 2011; Ye, et al., 2015). Sub-regional boundaries and their names show in cyan except for Rongbuk Catchment and Bolch's research of interest (Fig. 1). Kangxiong and Ngozumpa are also the names for the two glaciers. The debris covering rates varies from 3.7% to 47.2% for the eight sub-regions and the total debris covering rates is 17.7%. With an area of 73.215 km^2, Rongbuk glacier is the largest glacier in our study site and was combined by the middle Rongbuk and the western Rongbuk glacier. Different studies identify ELA (equilibrium line altitude) spans from 5430 ~ 6200 m, generally glaciers at the northern slope have higher ELA than the glaciers at the southern slope (King, et al., 2017). Meteorological records at the southern slope between 2660 and 5600 m suggested the temperature increased at 0.53 °C per decades and at the Dingri meteorological station suggested temperature increasing rates at 0.36°C per decades in the northern slope with a stronger increasing trend for the winter season (Bolch, et al., 2011; Salerno, et al., 2015).

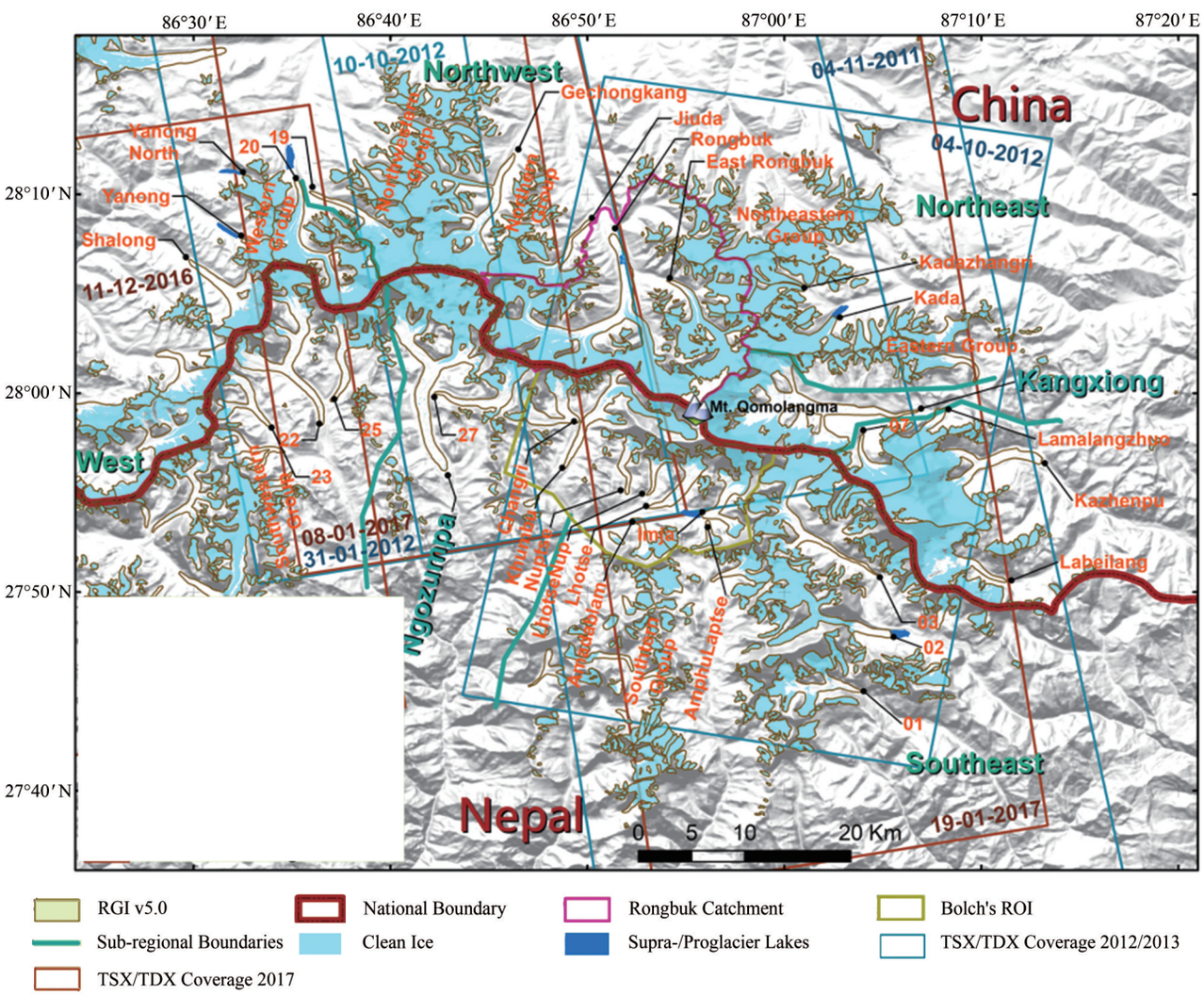

Fig.1 Study area and TSX/TDX images coverage

3 DATA

RGI v5.0 (RGI Consortium, 2015) outline is regarded as glacier boundary in this study except for several lacustrine-terminated glaciers that retreated significantly after 2000. RGI v5.0 outlines for most glaciers in this area are identified according to the Landsat image observed on 2000-10-30, which we also applied for clean-ice and debris-covered ice boundary identification. To correct the boundary of rapid retreated lacustrine-terminated glaciers, we obtained several Landsat images (2000-10-30, 2004-12-04, 2007-01-27, 2010-04-09, 2013-12-29, 2015-07-12 and 2017-12-08) for manually modifying outlines and positions basing on false-color images (SWIR: R, NIR: G, Red: B). We applied the RGI v5.0 outlines modified by the Landsat observations in 2007-01-27 and 2015-07-12 as average glacier outlines to calculate the glacier mass balance for the period before and after ~2013.

C-band SRTM DEM, observed in February of 2000, with a 1 arc-second (30 m) resolution was chosen as the reference DEM for the geocoding step in forming TanDEM-X DEM. As the void area was not fully filled for the 1 arc-second SRTM dataset, we employed void-filled in 3 arc-second (90 m) resolution C-band SRTM to fill the void for convenience in the InSAR processing. The void information of non-void filled SRTM dataset was employed for post-processing after InSAR procedure to mask out area was not real SRTM observation in 1 arc-second SRTM DEM. We compared C-band SRTM and X-band TanDEM-X DEM for deriving geodetic glacier mass balance between 2000 and ~2013. We followed Li, et al's (2018) research to evaluate and remove the possible penetration depths differences between C- and X-band by presuming that penetration depth differences between the X-band SRTM and TanDEM-X DEM can be waived (Rignot, et al., 2011). The penetration depth differences between two epochs of TanDEM-X DEM was waived as well despite a possible penetration depth of 4 m at the dry snow zone (Dehecq, et al., 2016). All acquisitions and SRTM used in this study were observed in the winter season to avoid possible seasonal fluctuation of glacier mass balance and/or penetration depth difference induced by snow covering changing.

TSX/TDX datasets in this research were observed in the bistatic model, which means one satellite (master satellite) transmits the pulses and two satellites receive the pulses almost simultaneously. TSX/TDX images were provided by the German Aerospace Center (DLR) in the Co-registered Single Look Slant Range Complex (CoSSC) format. The resolution of TSX/TDX images is around 2.5 m in both azimuth (along the flight direction) and ground range (across the flight direction). The TSX/TDX images used for this study were obtained in two different epochs one in 2011/2012, and other in 2016/2017. Since not much accumulation nor melting are supposed to occur in winter season, and SRTM performed in February, most TSX/TDX images selected in this study were observed in winter. We treated acquisition at the end of one year equally to the acquisition at the beginning of next year. For instance, the acquisitions on 2016-12-11 was regarded as the observation for winter of 2017. The detail information for the TSX/TDX images is listed below in Table 1 and Fig. 1 presents the coverage of the TSX/TDX in the study area.

Table 1 The specification of the TSX/TDX acquisitions

Date	Relative orbit	Orbital Pass	Effective perpendicular baseline/m	Height of ambiguity/m	Average incidence angle	Master satellite
2011−11−04	128	Ascending	113.8	−49.9	36	TSX
2012−01−31	128	Ascending	83.2	−62.9	34	TSX
2012−10−04	29	Descending	88.1	71.5	39	TSX
2012−10−10	128	Ascending	195.5	−28.0	35	TSX
2016−12−11	37	Ascending	117.7	70.9	48	TDX
2017−01−08	128	Ascending	117.1	44.6	34	TDX
2017−01−19	128	Ascending	117.3	48.4	36	TDX

4 METHODS

4.1 Bistatic D-InSAR

We followed a D-InSAR data processing to derive glacier height changes for the period of 2000 - ~2013 following Li, et al.'s (2018) research. The advantage of applying D-InSAR method other than directly performing DEMs differencing is that unwrapping is more stable since removing topographic phased reduced the phase gradient (Neckel, et al., 2013; Li & Lin, 2017). After removing the flat earth and topographic phase evaluated by TSX/TDX orbital information and SRTM, the rest is the topographic residual phase, which mainly induced by glacier height changes. After phase unwrapping, the topographic residual phase can be transferred to height changes for the next geocoding step. We presumed that no height changes occurred at the off-glacier area in the whole TSX/TDX coverage. Since notable glacier height changes might have occurred during our study period, the look-up table between the SAR and the geographic coordinates might not be accurate. Therefore, the evaluation of the topographic phase of SRTM could not be accurate as well. We performed the D-InSAR processing iteratively to generate TSX/TDX, each iteration generates a new TanDEM-X DEM (reference DEM plus topographic residual), which was applied as the reference DEM for next iteration. We stopped in the third iteration when usually the topographic residual phase was almost zero. In the third iteration, we added the evaluated topographic residual to the reference DEM to generated the final TanDEM-X DEM for the specific TSX/TDX acquisition. We removed area with strong geometry distortion. Then all the TanDEM-X DEM formed with single TSX/TDX acquisitions of ~2013 were mosaicked for next processing. All TSX/TDX were treated equally weighted in the overlapping area. The mosaicked TanDEM-X DEM minus the SRTM gives the height changes between 2000 and ~2013.

We proposed two processing procedures to derive glacier height changes for the period of ~2013 to 2016/2017. The first procedure is similar to Liu, et al's (2016) research for the Puruogangri Ice Field. We generated the mosaicked TanDEM-X DEM of 2016/2017 following the same procedure of processing of TSX/TDX ac-

quisitions of ~2013. Since both TanDEM-X DEM of ~2013 and 2016/2017 had been aligned to the same datum and projection of SRTM (WGS 84 and Longitude/Latitude in this study), differencing operation gives the height changes between ~2013 and 2016/2017. The second procedure was to regard the TanDEM-X DEM of ~2013 as the reference DEM and perform D-InSAR processing to the three TSX/TDX acquisitions of 2016/2017. Despite the short temporal interval of four to five years, which implies smaller height changes than one-decade time, an iterative D-InSAR was still applied as there were observable topographic residual phase in the second iteration. After the third iteration, the final TanDEM-X DEM of 2016/2017 was mosaicked with the three single frames. Glacier height changes between ~2013 and 2016/2017 was generated by make differencing of the TanDEM-X DEM of the two epochs.

4.2 Evaluating penetration differences

The possible penetration differences between C- and X-band were evaluated by comparing C- and X-band SRTM given they were the only available dataset which observed simultaneously for such purpose. Consider that X-band SRTM operates in strip map mode and failed to cover most parts of our study area, we adopted an adjacent region for such evaluation following Li, et al. (2018). Penetration depth differences and or penetration depth at debris-covered parts of the glaciers were presumed as zero. Clean ice boundary was identified according to Landsat images observed on 2000-10-30 and RGI v5.0. After radiometric and atmospheric correction, pixels with NDSI great than 0.4 and within the RGI v5.0 were identified as clean-ice. Height system are different for C- and X-band SRTM distribution, the former is orthometric height and the latter is ellipsoidal height. We presumed in this small area the geoid height was a ramp and the height different should be zero at off-glacier area. Since the orbital error of X-band SRTM was not perfectly corrected, we divided this area into two patches according to the orbital tracks for evaluating the systematic difference between C- and X-band SRTM (Marschalk, et al., 2004; Li, et al., 2018).

4.3 Miscellaneous

TSX/TDX acquisitions applied in this study observed in late autumn and in winter, and SRTM was operated in February. Consider most precipitation in the mid-Himalaya occurred in summer and the cold weather in winter, both activities of glacier mass accumulation and melting should be weak in winter, we presumed that no seasonal effects in this study. After removing the evaluated penetration depth differences, glacier height changes of the first period for each pixel were obtained. Basing on the temporal interval for each pixel, total glacier height changes were transferred to annual glacier height changes. Although the bistatic InSAR advantages in observing the accumulation zone, there were void areas due to geometry distortion, geometry decorrelation, and/or other reasons. We binned the glacier height changes in every 50m elevation and to fill the void area with the average value in each bin. By presuming that the glacier density of 850 ± 60kg/m^3, the annual glacier height changes were transferred to geodetic glacier mass balance (Huss, et al., 2013).

The accuracy estimation for period of 2000 to ~2013 followed Li, et al's (2018) instruction. For the evaluating glacier mass balance between ~2013 and 2016/2017 derived with both procedures, the error consisted of systematic error and random parts. The former part was composed by datum error and seasonal error, while the latter was contributed by error of the formed DEMs. The datum error was calculated with Eq. 1:

$$Err_{datum} = \frac{\sigma_{bi2017-bi2013(Off)}}{\sqrt{N_{Eff_{bi2017-bi2013(Off)}}}} \quad (1)$$

where $\sigma_{bi2017-bi2013(Off)}$ was the standard deviation of height differences in the off-glacier region. $\sqrt{N_{Eff_{bi2017-bi2013(Off)}}}$ was the effective measurement number which determined by the area of the off-glacier area and autocorrelation distance. Using variogram analysis, the autocorrelation distance was determined as 500 m for DEM difference map between SRTM and TanDEM-X DEM, and 200 m for the DEM difference map between TanDEM-X DEMs. Although we presumed that no seasonal effects for both glacier mass balance evaluation and penetration depth differences, 0.15m/month was still introduced for comparing DEM observed in difference months (Gardelle, et al., 2013). The random part was evaluated by equation 2:

$$Err_{random} = \frac{\sigma_{bi2017-bi2013(On)}}{\sqrt{N_{Eff_{bi2017-bi2013(On)}}}} \quad (2)$$

where $\sigma_{bi2017-bi2013(On)}$ was standard deviation of the height differences in the glacierized area. Since it cannot presume glacierized area was stable and not in-situ observation was available, we evaluated $\sigma_{bi2017-bi2013(On)}$ according to $\sigma_{bi2017-bi2013(Off)}$ by presuming the accuracy of DEM is correlated with slope rate. Standard deviation was calculated in seven bins in the off-glacier region including, 0-5, 5-10, 10-20, 20-30, 30-40, and >50°. Then we calculated proportion of glacierized area as weight calculate $\sigma_{bi2017-bi2013(On)}$.

5 RESULTS AND DISCUSSION

For results of the period between 2000 and ~2013 can refer to Li, et al.'s (2018) research with detail information. The observed geodetic glacier mass balance was -0.38 ± 0.04 m w.e. a^{-1}, which was similar to the world average level (Gardner, et al., 2013). Everest and its surroundings presented a spatial heterogeneous glacier height change pattern which possibly reflects debris-covering rates, terminating type, temperature rising rates, and glacier flow rates. Between 5000m and 6600m for the northern slope, and between 5000m and 6200m for the southern slope, the glacier height changes were almost linearly correlated with the elevations.

For the period between ~2013 and 2016/2017, the two data processing procedures yield with similar results in terms of average geodetic glacier mass balance and glacier height changing map. The average geodetic glacier mass balance was -0.512 ± 0.051 m w.e. a^{-1}, and -0.467 ± 0.048 m w.e. a^{-1} for the first and second procedures, respectively. Their discrepancy of value could be mainly due to orbital error correction and determination of the datum.

The standard deviation at off-glacier region is a key value for error propagation of accuracy estimation, which determines the datum error in both systematic part and random part. The standard deviations were 2.612 m and 2.168 m for the off-glacier region of the height change maps that derived from the first and second procedures, respectively. The standard deviation was similar to study of two TanDEM-X DEM differencing at the Puruogangri (Liu, et al., 2016), and much better than the SRTM and TanDEM-X differencing at the Everest (Li, et al., 2018). The first height change map was calculated from two DEMs differencing processing, while the second was the result of one D-InSAR processing, which means the first procedure performed adaptive power spectrum filtering independently for two D-InSAR processing and the second procedure performed the filtering operation only once. This could be the possible explanation for a greater standard deviation for the first procedure. In the rest parts of the paper, we adopt the results yield from the glacier height changing map derived from the second procedure.

Almost all sub-regions presented higher glacier mass lost rates during ~2013 and 2016/2017 than the first decade of 21st century (Li, et al., 2018). In table 2, we compared our derived geodetic glacier mass balance for two period before and after ~2013 for the entire study area and each sub-region.

Table 2 A comparison of the derived geodetic glacier mass balance（m w.e. a^{-1}）before and after ~2013

Region or sub-region	2000 to ~2013	~2013 to 2016/2017
Total region	−0.38 ± 0.04	−0.467 ± 0.048
Chinese Side（Northern slope）	−0.35 ± 0.04	−0.401 ± 0.050
Nepalese Side（Southern slope）	−0.41 ± 0.05	−0.587 ± 0.058
Southeast	−0.28 ± 0.05	−0.503 ± 0.054
Kangxiong	−0.13 ± 0.04	−0.417 ± 0.053
Northeast	−0.22 ± 0.04	−0.468 ± 0.053
Rongbuk Catchment	−0.51 ± 0.05	−0.588 ± 0.059
Northwest	−0.19 ± 0.04	−0.121 ± 0.042
West	−0.51 ± 0.05	−0.510 ± 0.047
Ngozumpa	−0.43 ± 0.05	−0.482 ± 0.054
Bolch's ROI	−0.48 ± 0.05	−0.758 ± 0.070

Northwest seemed to be the only sub-region presented with less glacier lost rate among the Mt. Everest and its surroundings. The Nepalese side experienced a larger acceleration of glacier mass loss rate than the Chinese side, which seemed to be a continuous trend since the last few decades of the 20th century (Li, et al., 2018). Kangxiong and Northeast sub-region presented less glacier mass loss rates than the regional average before ~2013, however after ~2013 their glacier mass loss rates were almost as equal as of the regional average. Rongbuk catchment and Bolch's ROI are two regions that have long period of historic geodetic glacier mass balance records, which presented with a steady trend of speeding up for the glacier mass lost despite slight discrepancy among different studies (Bolch, et al., 2011; Ye, et al., 2015; Li, et al., 2018). Compare to previous studies, our derived result found that the acceleration of glacier mass loss rate still kept after ~2013 and was more severe in the southern slope than in the northern despite much higher debris cover percentage (47.2% versus 12.1%) for Bolch's ROI.

The glacier height change map for ~2013 to 2016/2017 (Fig. 2) was almost identical as for the period of 2000 to ~2013 (Li, et al., 2018). The most significant glacier height changes during both periods occurred at the Gyabrag glacier (Unnamed 20 in Fig. 1, GLIMS ID G086590E28121N). Three independent studies yield similar glacier height changing map using SRTM as reference DEM (Gardelle, et al., 2013; King, et al., 2017; Li, et al., 2018). Given that almost no other available recent glacier height changing information was available for this site, it was reasonable to suspect the absurd large glacier height changes was due to the error of the common reference DEM (SRTM for this case). The two epochs of TSX/TDX derived glacier height change maps also found the most obvious changes occurred at the Gyabrag glacier almost confirmed us this phenomenon, which requires further investigation for its trigger factors.

We analyzed glacier height changes in every 50 m elevation bin for each sub-region (Fig. 3). Given the difference of glacier elevation distributions and their ELAs between the northern and southern side, glacier height changes histogram was not show for total region. Before ~2013 at the Chinese side, the glacier height changing rates were almost linear to elevation from 5200 m to 6600 m before ~2013, while after ~2013 more glacier height downwasting occurred below 6000 m. For the Nepalese side, more downwasting occurred from ~5000 m to 6400 m where distribute almost all clean ice glaciers. To align off-glacier area in the vertical direction when comparing two DEMs for deriving glacier height changes is the key step. The integral bias might have occurred when off-glacier regions were not perfectly aligned. In this study, according to the height changing rate in each 50 m elevation bin, the acceleration of melting occurred at lower area and implied that great negative lost rates should not be due to wrongly alignment of the off-glacier area in the vertical direction.

The quick expansion of proglacial lake was a sign of the quick glacier mass losing. Unnamed 02, Yanong North, Yanong, Kada, and Imja glacier were identified as lacustrine-terminating glaciers in this area. Since the quick expansion of the Rongbuk lake, we take the Rongbuk glaciers into analysis as well. Their glacier mass balance for these glaciers during 2000 and ~2013 was -0.51 ± 0.05 m w.e. a^{-1}, comparing to the local average of 0.38 m w.e. a^{-1} (Li, et al., 2018). For after ~2013, the geodetic glacier mass balance was -0.659 ± 0.053 m w.e. a^{-1} which was still greater than the regional average. In fig. 4 we present the glacier terminus retreatment for these five lacustrine-terminating glaciers.

Despite there is almost no in-situ observations in terms of glacier height changes or mass balance in either Chinese or Nepalese side given its hash environment and remote, glacier mass lost rate acceleration was reported along the Himalayan by comparing three DEM observed in different time including KH-9 Hexagon film (1975), SRTM (2000) and ASTER (2016), which also report the discrepancy of glacier mass lost rates among clean-ice glaciers, debris-covered glaciers, and lacustrine-terminating glaciers (Maurer, et al., 2019). By using TSX/TDX imagery observed from 2011—2016 and similar data processing method to this study, accelerated glacier mass loss over the Puruogangri ice field in the inner Tibetan Plateau (Liu, et al., 2019). Surface runoff observation could be an alternative method for validating the acceleration of glacier mass lost as gauge station observation in the Rongbuk basin found that glacier melting dominated the annual runoff (Ye, et al., 2015).

6 CONCLUSION

In this study, we explored the capability of deriving sub-decadal geodetic glacier mass balance by bistatic SAR Interferometry. Two data processing procedures were promoted and tested for such purpose, one was to form two independent DEMs by performing topography differencing. The other was to form one DEMs and regarding as reference topography to performing a D-InSAR procedure. The second processing strategy presents a higher precision. The error in estimating 4—5 years geodetic glacier mass balance by using two epochs of TerraSAR-X/TanDEM-X acquisitions was similar to one-decade geodetic glacier mass balance by using SRTM and TerraSAR-X/TanDEM-X. Glaciers at the Mt. Everest experienced speeding up of glacier mass loss after ~2013. The acceleration at the southern slope was greater than at the northern slope. The spatial heterogenous glacier downwasting pattern for after ~2013 was similar to before ~2013. Lacustrine-terminating glaciers experienced more rapid loss rates than regional average in associate with notable terminus retreat.

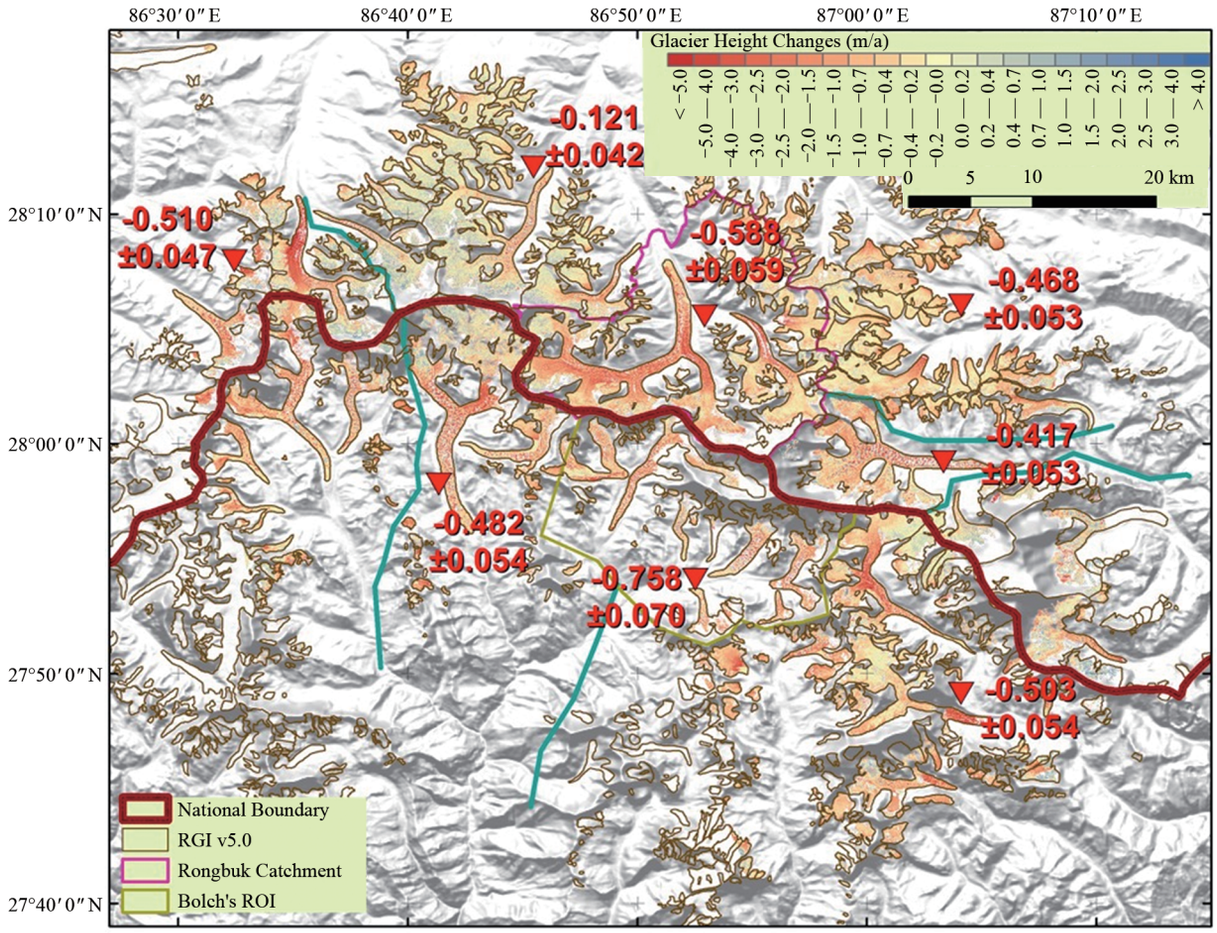

Fig.2 Annual glacier height change maps and sub-region glacier mass balance (in numbers) at the Everest and its surrounding for ~ 2013 to 2016/2017.

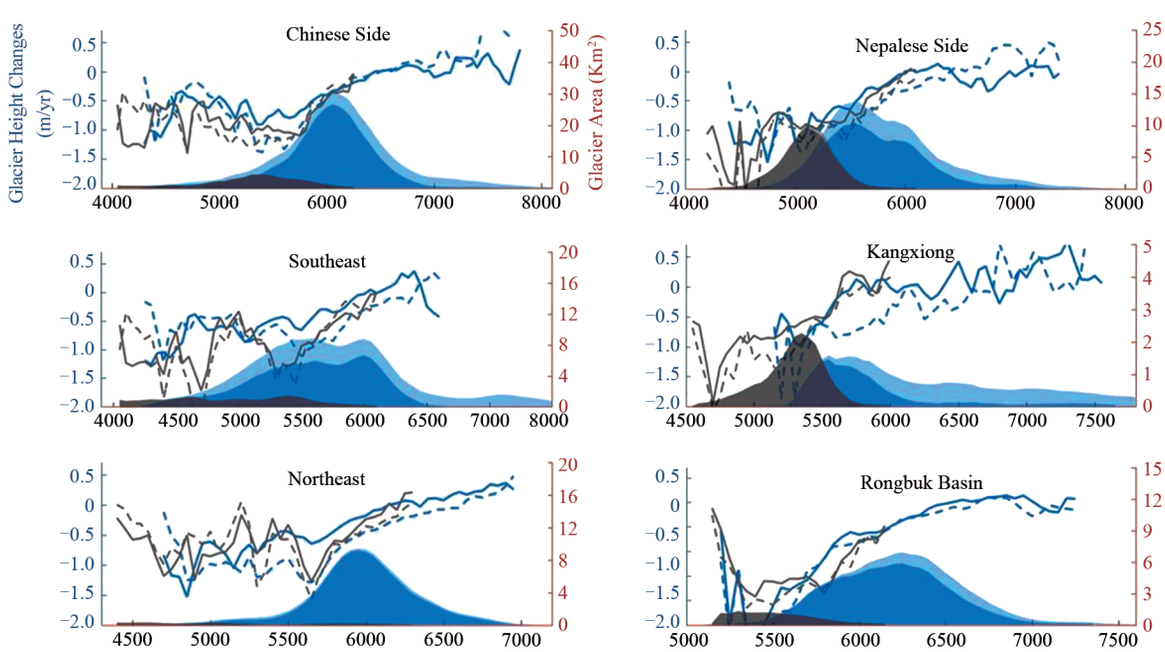

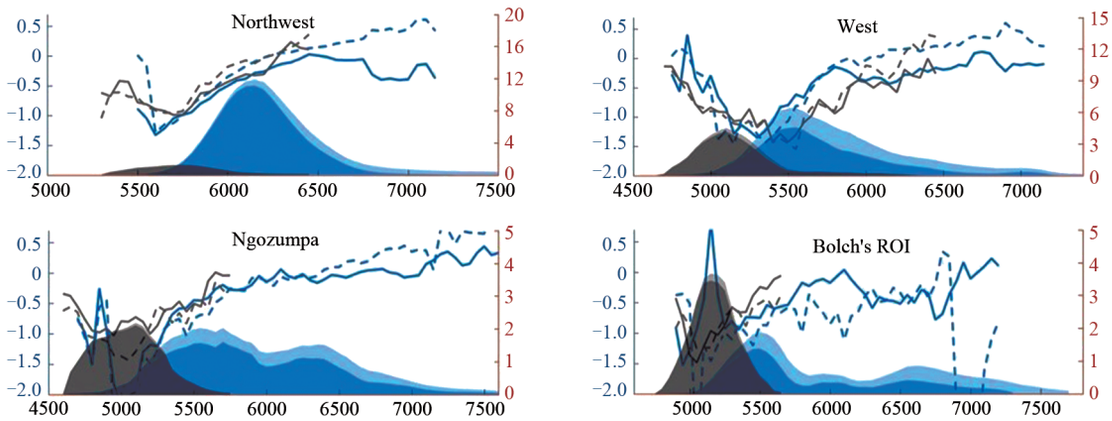

Fig.3 Glacier height change rates at different elevations before (solid line) and after (dash line) ~2013. The filled area presents the measured glacierized area (dark parts) and the total glacierized area (light parts).

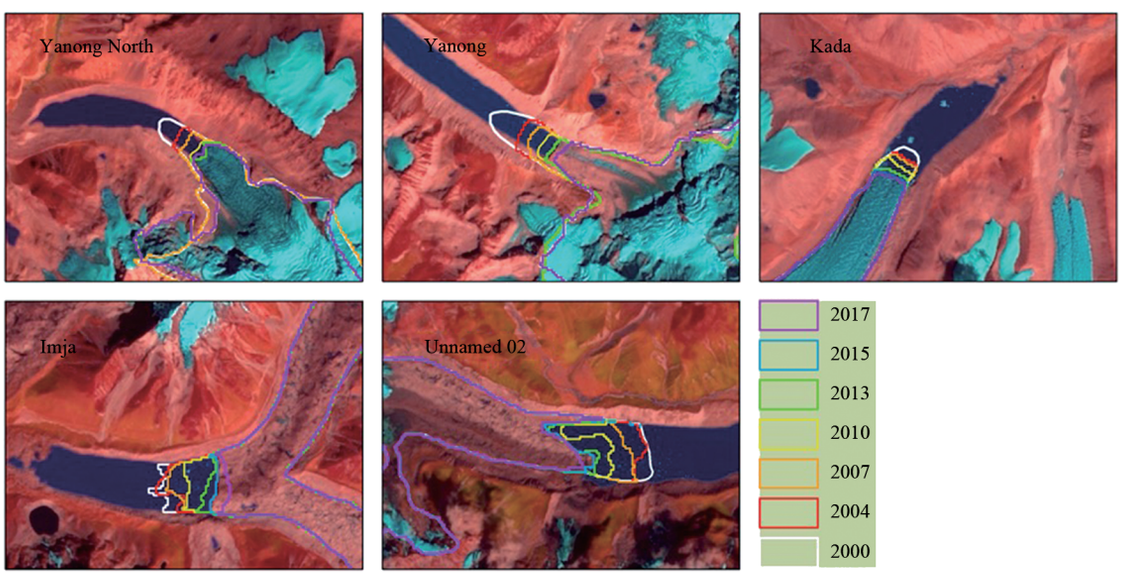

Fig.4 Retreating of lacustrine-terminating glaciers during years 2000 and 2017.

REFERENCES

Bolch T, Pieczonka T, and Benn D I. 2011. Multi-decadal mass loss of glaciers in the Everest area (Nepal Himalaya) derived from stereo imagery. The Cryosphere, 5, 349-358. DOI:10.5194/tc-5-349-2011

Dehecq A, Millan R, Berthier E, Gourmelen N, Trouvé E, and Vionnet V. 2016. Elevation changes inferred from TanDEM-X data over the Mont-Blanc area: Impact of the X-band interferometric bias. IEEE Journal of Selected Topics in Applied Earth Observations and Remote Sensing, 9(8), 3870-3882. DOI: 10.1109/JSTARS.2016.2581482

Farr T G, Rosen P A, Caro E, Crippen R, Duren R, Hensley S, Kobrick M, Paller M, Rodriguez E, Roth L, Seal D, Shaffer S, Shimada J, Umland J, Werner M, Oskin M, Burbank D, and Alsdorf. 2007. The shuttle radar topography mission. Reviews of geophysics, 45 (2). Doi:10.1029/2005RG000183

Gardelle J, Berthier E, Arnaud Y, and Kääb A. 2013. Region-wide glacier mass balances over the Pamir-Karakoram-Himalaya during 1999-2011. Cryosphere, 7, 1885-1886. DOI: 10.5194/tc-7-1263-2013

Kääb A, Treichler D, Nuth C, and Berthier E. 2015. Brief Communication: Contending estimates of 2003 – 2008 glacier mass balance over the Pamir – Karakoram – Himalaya. The Cryosphere, 9, 557-564. DOI:10.5194/tc-9-557-2015

King O, Quincey D J, Carrivick J L, and Rowan A V. 2017. Spatial variability in mass loss of glaciers in the Everest region, central Himalayas, between 2000 and 2015. The Cryosphere, 11(1), 407-426. DOI:10.5194/tc-11-407-2017

Krieger G, Zink M, Bachmann M, Bräutigam B, Schulze D, and Martone M. 2013. TanDEM-X: A radar interferometer with two formation-flying satellites. Acta Astronautica, 89, 83-98. DOI: 10.1016/j.actaastro.2013.03.008

Li G, and Lin H. 2017. Recent decadal glacier mass balances over the Western Nyainqentanglha Mountains and the increase in their melting contribution to Nam Co Lake measured by differential bistatic SAR interferometry. Global and Planetary Change, 149, 177-190. DOI:10.1016/j.gloplacha.2016.12.018

Li G, Lin H, and Ye Q. 2018. Heterogeneous decadal glacier downwasting at the Mt. Everest (Qomolangma) from 2000 to~ 2012 based on multi-baseline bistatic SAR interferometry. Remote Sensing of Environment, 206, 336-349. DOI:10.1016/j.rse.2017.12.032

Liu L, Jiang L, Sun Y, Yi C, Wang H, and Hsu H. 2016. Glacier elevation changes (2012 – 2016) of the Puruogangri ice field on the Tibetan Plateau derived from bi-temporal TanDEM-X InSAR data. International Journal of Remote Sensing, 37, 5687-5707. DOI:

10.1080/01431161.2016.1246777

Liu L, Jiang L, Jiang H, Wang H, Ma N, Xu H. 2019. Accelerated glacier mass loss (2011 – 2016) over the Puruogangri ice field in the inner Tibetan Plateau revealed by bistatic InSAR measurements. Remote Sensing of Environment, 231: 111241. DOI: 10.1016/j.rse.2019.111241

Marschalk U, Roth A, Eineder M, and Suchandt S. 2004. Comparison of DEMs derived from SRTM/X-and C-Band. 2014 IEEE International Geoscience and Remote Sensing Symposium, 2004, 4531-4534. DOI: 10.1109/IGARSS.2004.1370162

Maurer J M, Schaefer J M, Rupper S, and Corley A. 2019.Acceleration of ice loss across the Himalayas over the past 40 years. Science advances, 5(6): eaav7266. DOI: 10.1126/sciadv.aav7266

Neckel N, Braun A, Kropáček J, and Hochschild V. 2013. Recent mass balance of the Purogangri Ice Cap, central Tibetan Plateau, by means of differential X-band SAR interferometry. Cryosphere, 7, 1623-1633. DOI: 10.5194/tc-7-1623-2013

Rignot E, Echelmeyer K, and Krabill W. 2001. Penetration depth of interferometric synthetic - aperture radar signals in snow and ice. Geophysical Research Letters, 28, 3501-3504. DOI: 10.1029/2000GL012484

ConsortiumRGI. 2015. Randolph Glacier Inventory – A Dataset of Global Glacier Outlines: Version 5.0: Technical Report, Global Land Ice Measurements from Space, Colorado, USA. Digital Media. DOI: 10.7265/N5-RGI-50

Salerno F, Guyennon N, Thakuri S, Viviano G, Romano E, Vuillermoz E, Cristofanelli P, Stocchi P, Agrillo G, Ma Y, and Tartari G. 2015. Weak precipitation, warm winters and springs impact glaciers of south slopes of Mt. Everest (central Himalaya) in the last 2 decades (1994 – 2013. The Cryosphere, 9, 1229-1247. DOI: 10.5194/tc-9-1229-2015

Ye Q, Zhong Z, Kang S, Stein A, Wei Q, and Liu J. 2009. Monitoring glacier and supra-glacier lakes from space in Mt. Qomolangma region of the Himalayas on the Tibetan Plateau in China. Journal of Mountain Science, 6, 211-220. DOI: 10.1007/s11629-009-1016-4

Ye Q, Bolch T, Naruse R, Wang Y, Zong J, Wang Z, Zhao R, Yang D, and Kang S. 2015. Glacier mass changes in Rongbuk catchment on Mt. Qomolangma from 1974 to 2006 based on topographic maps and ALOS PRISM data. Journal of Hydrology, 530, 273-280. DOI: 10.1016/j.jhydrol.2015.09.014